Thickness dependence of dielectric constant of alumina films based on first-principles calculations

Cite as: Appl. Phys. Lett. 121, 062902 (2022); https://doi.org/10.1063/5.0106721 Submitted: 29 June 2022 • Accepted: 26 July 2022 • Published Online: 12 August 2022

Shogo Fukushima, Rajiv K. Kalia, D Aiichiro Nakano, et al.













Thickness dependence of dielectric constant of alumina films based on first-principles calculations

Cite as: Appl. Phys. Lett. **121**, 062902 (2022); doi: 10.1063/5.0106721 Submitted: 29 June 2022 · Accepted: 26 July 2022 · Published Online: 12 August 2022







Shogo Fukushima,^{1,2} Rajiv K. Kalia,² Aiichiro Nakano,^{2,a)} (i) Fuyuki Shimojo,¹ (i) and Priya Vashishta² (i)

AFFILIATIONS

Department of Physics, Kumamoto University, Kumamoto 860-8555, Japan

ABSTRACT

Optoelectronic properties of devices made of two-dimensional materials depend largely on the dielectric constant and thickness of a substrate. To systematically investigate the thickness dependence of dielectric constant from first principles, we have implemented a double-cell method based on a theoretical framework by Martyna and Tuckerman [J. Chem. Phys. 110, 2810 (1999)] and therewith developed a general and robust procedure to calculate dielectric constants of slab systems from electric displacement and electric field, which is free from material-specific adjustable parameters. We have applied the procedure to a prototypical substrate, Al₂O₃, thereby computing high-frequency and static dielectric constants of a finite slab as a function of the number of crystalline unit-cell layers. We find that two and four layers are sufficient for the high-frequency and static dielectric constants of (0001) Al₂O₃ slabs to recover 90% of the respective bulk values computed by a Berry-phase method. This method allows one to estimate the thickness dependence of dielectric constants for various materials used in emerging two-dimensional nanophotonics, while providing an analytic formula that can be incorporated into photonics simulations

Published under an exclusive license by AIP Publishing. https://doi.org/10.1063/5.0106721

Dielectric screening by a substrate significantly modifies optoelectronic properties of devices made of two-dimensional (2D) materials deposited on it. Qiu et al. reported that the optoelectronic properties of few-layer black phosphorus on a substrate are sensitive to the species of the substrate such as sapphire (Al₂O₃) and hexagonal boron nitride (hBN). Optoelectronic properties, such as quasiparticle gap, optical gap, and exciton binding energy, are largely influenced by dielectric properties and surface structures of the substrates. In transition metal dichalcogenides (TMDs), it is well known that additional screening from a metallic graphene substrate or capping layer can reduce the quasiparticle bandgap. Bradley et al. reported that direct and indirect band gaps of few-layer MoSe2 can be reduced by 0.1-0.2 eV by additional bilayer graphene on a 6H-SiC(0001) substrate.² Raja et al. investigated the effects of graphene on dielectric constants and bandgaps of WS₂ and WSe₂ on SiO₂ and hBN substrates.³ They also reported that additional bilayer graphene reduces the bandgap by 0.13 eV. Such substrate screening should play a dominant

role in emerging nanophotonics based on 2D materials.^{4,5} In these applications, it is essential to accurately assess the dielectric constant of substrate as a function of its thickness, because dielectric constant of a finite slab often exhibits highly nontrivial thickness dependence.⁶

In the literature, several methods have been suggested for calculating dielectric constants of atomically thin 2D materials. Laturia *et al.* calculated dielectric constants of 2D materials such as hBN and TMDs from the principle of equivalent capacitance, using a dielectric constant of supercell computed from Born effective-charge tensor and force-constant matrix. Santos *et al.* suggested a method for calculating dielectric constants of slabs, by introducing a compensating electric field in vacuum area between polarized slabs due to periodic boundary condition. They calculated dielectric constants of few-layer MoS₂ under a finite electric field. In these methods, corrections were made to incorporate the effects of a vacuum layer on dielectric constant caused by periodic boundary conditions. However, it remains untested for thicker slabs whether these corrections can adequately eliminate

²Collaboratory for Advanced Computing and Simulations, Department of Physics and Astronomy, Department of Computer Science, Department of Chemical Engineering and Materials Science, Department of Quantitative and Computational Biology, University of Southern California, Los Angeles, California 90089-0242, USA

a) Author to whom correspondence should be addressed: anakano@usc.edu

Coulomb interaction between periodic images. Instead, we here focus on a general theoretical framework by Martyna and Tuckerman to explicitly eliminate Coulomb interaction between periodic images.9-They applied the framework to cluster (0D), wire (1D), and slab (2D) systems. 11 In their 2D method, long-range Coulomb interaction along the direction perpendicular to 2D surface is excluded in the Ewald summation. Hereafter, we call this method "double-cell method" because two types of supercells are used for the calculation of wave functions and long-range Coulombic interaction, respectively. Another serious problem is the sensitivity to material-specific adjustable parameters used to define the boundary between material and vacuum in existing methods. We have developed a simple method to calculate dielectric constants of slab systems from electric displacement and electric field, which is free from material-specific adjustable parameters. Accordingly, the method is generally applicable to other materials without any modification and robust, e.g., with respect to the presence

In this paper, we apply the double-cell method to a prototypical dielectric substrate, Al₂O₃, which is used widely, e.g., as substrate for femtosecond surface x-ray scattering of WSe₂. ¹³ sol–gel preparation of TiO₂ film, ¹⁴ room-temperature ferromagnetism of In₂O₃, ¹⁵ and metalorganic vapor-phase epitaxial growth of ZnO nanorods. ¹⁶ We calculate high-frequency and static dielectric constants of Al₂O₃ slabs and investigate their thickness dependence and convergence toward the respective bulk values, which, in turn, are computed using a Berry-phase method. ^{17,18} This paper describes step-by-step procedures that we have developed for computing thickness-dependent dielectric constants of slab systems based on the double-cell method and compares their computational efficiency with previously proposed methods. Moreover, we provide analytical formula that can be used in photonic simulations of thin slabs ¹⁹ such as increasingly available freestanding films. ^{20,21}

As a reference, we first compute dielectric constants in bulk system, for which several methods have been proposed. 17,18,22,23 In this study, we use the method proposed by Umari *et al.* for the treatment of homogeneous electric field within first principles calculations. 17,18 Generally, dielectric constant ε_{ω} depends on the frequency ω of the external electric field. For ω above the largest phonon frequency, we compute the high-frequency dielectric constant ε_{∞} including only electronic response. The ε_{∞} is calculated as

$$\varepsilon_{\infty} = 1 + 4\pi \frac{\Delta P_E}{F},\tag{1}$$

where ΔP_E is the change in polarization defined by Resta *et al.*²⁴ due to the finite electric field E for fixed atomic positions. In addition, we compute the static dielectric constant ε_0 , which includes both electronic and ionic responses. To include the ionic response, we take into account of atomic relaxation by performing structure optimization under the finite electric field. The ε_0 can then be obtained by including ionic contribution in ΔP_E .

Ewald method is commonly employed in the calculation of longrange Coulombic interaction when using periodic boundary condition. In order to exclude Coulomb interaction between periodic images, Martyna and Tuckerman suggested methods for calculating Coulomb energy if one or more dimensions are non-periodic. In their method, two types of supercells are used, i.e., a small cell to calculate the short-range energy contribution in the Ewald method as well as wave functions and electron density and a larger cell to evaluate the long-range energy contribution that excludes periodic-image artifact. ¹² In this study, we used this "double-cell method" to investigate dielectric properties of slab systems. The detailed description of the calculation method is provided in the supplementary material.

Dielectric constant is defined as the ratio between electric displacement D and electric field E. We obtain dielectric constants of slab systems by applying an external electric field $E_{\rm ext}$ and calculating D and E from local Kohn—Sham (KS) potential $V_{\rm loc}(z)$ along [0001] direction. Figure 1 shows the difference of $V_{\rm loc}(z)$ with and without the electric field for a slab of one-crystalline-unit-cell thickness

$$\Delta V_{\text{loc}}^{E}(z) = V_{\text{loc}}^{E}(z) - V_{\text{loc}}^{0}(z), \tag{2}$$

where $V^E_{\rm loc}(z)$ and $V^0_{\rm loc}(z)$ are the local KS potentials under finite electric field E and zero electric field, respectively. Red and blue lines in Fig. 1 represent $\Delta V^E_{\rm loc}(z)$ without and with atomic relaxation, which correspond to ε_∞ and ε_0 , respectively. Compared to vacuum $(0~{\rm \AA} < z < 5~{\rm \AA}, 20~{\rm \AA} < z < 25~{\rm Å})$, smaller slopes are observed in slab $(5~{\rm \AA} < z < 20~{\rm \AA})$ due to screening. D and E are calculated from the slope of $\Delta V^E_{\rm loc}(z)$ by linear fitting in vacuum and slab regions, respectively. We then calculate the dielectric constant as D/E. While an alternative method to determine the dielectric constant would use polarizations calculated by the double-cell method, which was found to be less effective (see the supplementary material).

The electronic states are calculated using the projector augmented-wave (PAW) method^{25,26} within the framework of a density functional theory (DFT). Projector functions are generated for the 3s and 3p states of aluminum (Al) and 2s and 2p states of oxygen (O). The generalized gradient approximation (GGA) is used for the exchange-correlation energy.²⁷ The momentum-space formalism was utilized, where the plane wave cutoff energies are 30 and 250 Ry for the electronic pseudo-wave functions and pseudo-charge density, respectively. $3 \times 3 \times 1$ k points are used for Brillouin-zone sampling for electronic-structure calculations in the slab system, with 3×3 k points in the lateral directions. An external electric field of $E_{\rm ext}=10^{-3}$ a.u. is applied, which is within the linear-response range (see the supplementary material). To investigate the dependence of ε_{∞} and ε_{0} on the number of layers n, we use the bulk system and slab system consisting of 1, 2, 3, 4, and 5 layers (referred to as 1L, 2L, 3L, 4L, and 5L systems) of the Al₂O₃ slab, as shown in Fig. 2, where the surfacenormal (z) direction is the crystallographic [0001] direction. The bulk system containing 120 atoms in an orthorhombic supercell is used with periodic boundary condition. The orthorhombic supercell size is

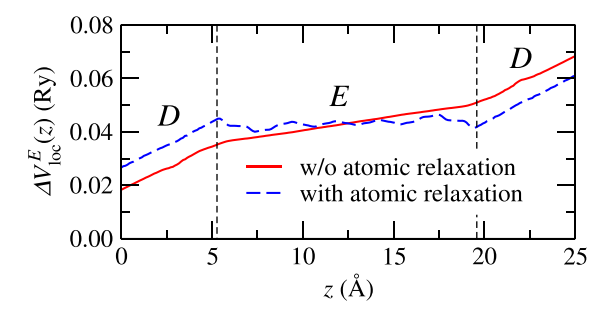


FIG. 1. Differences of local Kohn–Sham potential of a one-layer system with and without the electric field. Red and blue lines represent $\Delta V^{\mathcal{E}}_{\text{loc}}(z)$ without and with atomic relaxation, respectively.

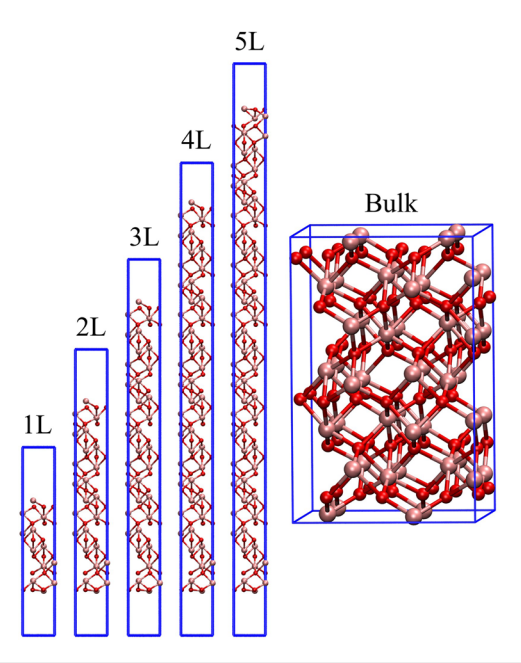


FIG. 2. Schematic of the simulation systems of Al₂O₃. Magenta and red spheres represent Al and O atoms, respectively, while blue lines represent edges of the sim-

 $9.668 \times 8.416 \times 13.189 \text{ Å}^3$. The 1L, 2L, 3L, 4L, and 5L slab systems containing 30, 60, 90, 120, and 150 atoms in a hexagonal supercell are used. The hexagonal 1L, 2L, 3L, 4L, and 5L supercells are set to be $4.900 \times 4.900 \times 25$ $4.878 \times 4.878 \times 37.5$, $4.861 \times 4.861 \times 50$, $4.856 \times 4.856 \times 62.5$, and $4.852 \times 4.852 \times 75 \text{ Å}^3$, respectively. These supercell sizes in x and y directions are decided so that the pressure becomes 0 GPa and that of z direction is decided by inserting vacuum regions of 5 Å in top and bottom of supercell in the z direction. Conventional periodic boundary conditions are used in x and y directions in the slab systems.

We first calculate the high-frequency and static dielectric constants, ε_{∞} and ε_0 , of the bulk system in three (x, y, and z) directions. It is known that dielectric properties of Al₂O₃ are anisotropic between vertical (\perp) and parallel (\parallel) directions to [0001].²⁸ ε_{∞} and ε_{0} vertical to [0001] are calculated by the average of x and y directions. Table I shows the obtained ε_{∞} and ε_0 in the present work, which are in good agreement with the previous work by Schubert et al.²⁹ These values should coincide with ε_{∞} and ε_{0} of slabs in the infinite-thickness limit.

As mentioned previously, dielectric constants are calculated by the ratio of D and E obtained from the slopes of $\Delta V_{loc}^{E}(z)$ in vacuum

TABLE I. High-frequency and static dielectric constants of Al₂O₃.

	Schubert et al. ²⁹	Present work
$E \perp [0001] \varepsilon_{\infty}$	3.077	2.937
ε_0	9.385 ± 0.013	9.561
$E\parallel [0001]$ ε_{∞}	3.072	3.061
$arepsilon_0$	11.61 ± 0.016	11.86

and slab, respectively. However, the dielectric constants, in particular, ε_0 , depend sensitively on the range of linear-fitting w due to the fluctuation of $\Delta V_{loc}^{E}(z)$ in slab and accordingly the estimated E value (see the blue line in Fig. 1). On the other hand, D obtained by linear fitting is insensitive to w and is almost the same as E_{ext} , as expected. Figure 3 shows ε_{∞} and ε_0 as a function of w, while the center of the range of the linear fitting is fixed at the center of the slab. Fluctuations of ε_{∞} are sufficiently small for all systems, while those of ε_0 are larger. In particular, fluctuation of ε_0 for 1L system is too large to determine a unique value, whereas those for 2, 3, 4, and 5L systems converge as w increases. For statistical estimation while excluding the effects of surface, the dielectric constants and their error bars are obtained from the average and standard deviation at 50% $< w/d_n^{\rm slab} < 80$ %, where $d_n^{\rm slab}$ is the thickness of the *n*-layer slab system.

Figure 4 shows the calculated ε_{∞} and ε_{0} as a function of n. 1L system is an outlier, since the statistical errors of ε_{∞} and ε_{0} of are much larger than those of the other systems. On the other hand, ε_{∞} and ε_0 of 2, 3, 4, and 5L systems monotonically increase as a function of n. Convergence to the bulk value can be fitted to the following analytical formula:

$$\varepsilon_{\infty} = \varepsilon_{\infty, [0001]}^{\text{bulk}} - \frac{a}{n+b},$$

$$\varepsilon_{0} = \varepsilon_{0, [0001]}^{\text{bulk}} - \frac{c}{n+d},$$

$$(3)$$

$$\varepsilon_0 = \varepsilon_{0,[0001]}^{\text{bulk}} - \frac{c}{n+d},\tag{4}$$

where $\varepsilon_{\infty,\,[0001]}^{\text{bulk}}$ and $\varepsilon_{0,\,[0001]}^{\text{bulk}}$ are the high-frequency and static dielectric constants of bulk in [0001] direction, whereas a, b, c, and d are fitting parameters (a = 7.241, b = 33.39, c = 9.165, and d = 3.679). The fit reasonably describes the *n*-dependence of ε_{∞} and ε_0 , which converges to respective bulk values. According to these thickness dependences, ε_{∞} and ε_{0} of the slab system have exceeded 90% of the corresponding bulk values at 2 and 4 layers, respectively. These thickness dependences allow us to estimate the dielectric constants of finite-layered alumina and predict their effects on optoelectronic properties when it is used as a substrate. Thickness dependence was observed experimentally for the dielectric constant of alumina films. 30,31 While commonly observed dielectric constant values increase with the thickness of the

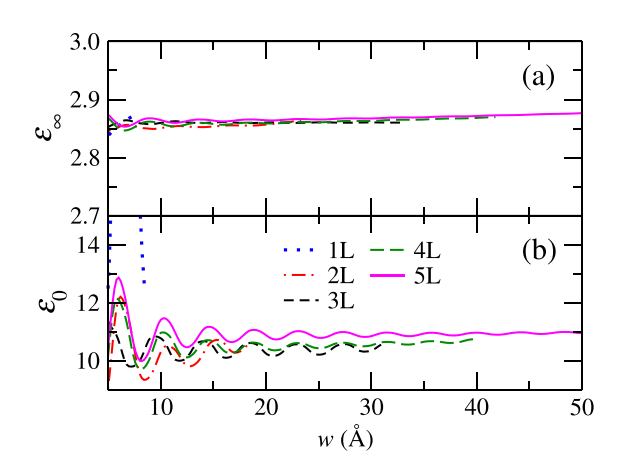


FIG. 3. (a) High-frequency and (b) static dielectric constants as a function of the range w of linear fitting. Blue, red, black, green, and magenta lines represent the dielectric constants of 1, 2, 3, 4, and 5L systems, respectively.

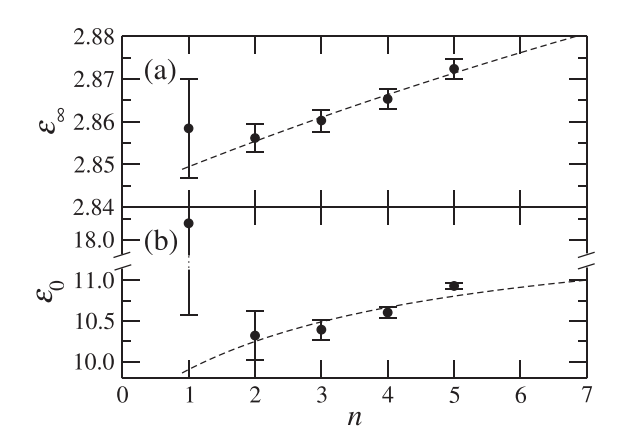


FIG. 4. (a) High-frequency and (b) static dielectric constants as a function of the number of layers n. Dashed lines show the best fits [Eqs. (3) and (4)].

Al₂O₃ film down to 200 Å, ³⁰ a previous study reported a dielectric constant ($\epsilon_0 \sim 11$) for thin (10–50 Å) Al₂O₃ atomic layer deposition (ALD) films. ³² Nevertheless, it is experimentally highly challenging to measure the dielectric constant of isolated thin slabs without substrate effects. In addition, thin Al₂O₃ films in experiments are usually amorphous, and it is reported that the dielectric constant of amorphous Al₂O₃ (\sim 8.0) is lower than the crystalline value (\sim 12.0). ³³ Because we consider perfect crystalline slab, the calculated values tend to be higher than experimental values on amorphous ALD films.

Experimentally, dielectric constants of ultrathin alumina films are affected by contacts with other materials. 30,34 Such interfacial systems can have defects and varying coordination numbers. 35 We have thus investigated effects of surface defects on dielectric constants. The calculated $\Delta V_{\rm loc}^E(z)$ with oxygen vacancies are nearly the same as those of perfect structures as shown in Fig. S5 in the supplementary material. These results confirm that the proposed method is robust with respect to the presence of defects.

Finally, we compare the computational efficiency and robustness of the proposed method with those of previously suggested methods. We first examine supercell-size dependence of ε_0 calculated based on an alternative method proposed by Santos $et~al.^8$ (see Fig. S1 in the supplementary material). However, the calculated ε_0 depends significantly on the supercell size, especially for thin slabs. This is contrary to the double-cell method proposed in this work, which gives supercell size-independent polarization of an isolated slab without the use of excessively large supercells, as shown in Fig. S2. We have also tested an alternative method to calculate the thickness dependence of ε_0 through polarization using Eq. (1), but it produces incorrect behavior as shown in Fig. S3. These comparisons with alternative methods to calculate dielectric constants confirm the computational efficiency and robustness of our method.

In summary, we have developed a robust procedure to determine thickness-dependent dielectric constants of slabs from first principles based on a double-cell method and applied it to $\mathrm{Al_2O_3}$. The calculated high-frequency and static dielectric constants as a function of the number of layers monotonically converge to respective bulk values computed by the Berry-phase method. It was estimated that 2 and 4 layers are sufficient, respectively, for the high-frequency and static dielectric constants to recover 90% of bulk values. We have also

provided accurate analytical formula, Eqs. (3) and (4), which can be used in photonic simulations of thin slabs.

See the supplementary material for detailed descriptions of Berry-phase and double-cell methods, comparison with alternative calculation methods in Figs. S1–S3, linear dependence on the electric field in Fig. S4, and the effects of surface defects on dielectric constant in Fig. S5.

This study was supported by JSPS KAKENHI (Grant Nos. 21J10836 and 21H01766) and JST CREST (Grant No. JPMJCR1812), Japan. The work at the University of Southern California was supported by the National Science Foundation, Future Manufacturing Program (Award No. NSF 2036359). The authors thank the Supercomputer Center, the Institute for Solid State Physics, University of Tokyo, for the use of the facilities. The computations in this work were also performed using the facilities of the Research Institute for Information Technology, Kyushu University.

AUTHOR DECLARATIONS Conflict of Interest

The authors have no conflicts to disclose.

Author Contributions

Shogo Fukushima: Conceptualization (equal); Funding acquisition (equal); Investigation (equal); Supervision (equal); Validation (equal); Visualization (equal); Writing – original draft (equal); Writing – review and editing (equal). Rajiv K. Kalia: Funding acquisition (equal); Investigation (equal); Resources (equal); Validation (equal); Visualization (equal); Writing – original draft (equal); Writing – review and editing (equal). Aiichiro Nakano: Conceptualization (equal); Funding acquisition (equal); Resources (equal); Supervision (equal); Writing – original draft (equal); Writing – review and editing (equal). Fuyuki Shimojo: Conceptualization (equal); Writing – original draft (equal); Writing – review and editing (equal). Priya Vashishta: Project administration (equal); Writing – original draft (equal); Writing – review and editing (equal).

DATA AVAILABILITY

The data that support the findings of this study are available from the corresponding author upon reasonable request.

REFERENCES

¹D. Y. Qiu, F. H. da Jornada, and S. G. Louie, Nano Lett. 17(8), 4706 (2017).

²A. J. Bradley, M. M. Ugeda, F. H. da Jornada, D. Y. Qiu, W. Ruan, Y. Zhang, S. Wickenburg, A. Riss, J. Lu, S. K. Mo, Z. Hussain, Z. X. Shen, S. G. Louie, and M. F. Crommie, Nano. Lett. 15(4), 2594 (2015).

³A. Raja, A. Chaves, J. Yu, G. Arefe, H. M. Hill, A. F. Rigosi, T. C. Berkelbach, P. Nagler, C. Schuller, T. Korn, C. Nuckolls, J. Hone, L. E. Brus, T. F. Heinz, D. R. Reichman, and A. Chernikov, Nat. Commun. 8, 15251 (2017).

⁴A. B. Khanikaev and G. Shvets, Nat. Photonics 11(12), 763 (2017).

⁵M. Turunen, M. Brotons-Gisbert, Y. Dai, Y. Wang, E. Scerri, C. Bonato, K. D. Jöns, Z. Sun, and B. D. Gerardot, Nat. Rev. Phys. 4(4), 219 (2022).

⁶M. Stengel and N. A. Spaldin, Nature **443**(7112), 679 (2006).

⁷A. Laturia, M. L. Van de Put, and W. G. Vandenberghe, npj 2D Mater. Appl. 2(1), 6 (2018).

⁸E. J. G. Santos and E. Kaxiras, ACS Nano 7(12), 10741 (2013).

- ⁹G. J. Martyna and M. E. Tuckerman, J. Chem. Phys. **110**(6), 2810 (1999).
- ¹⁰P. Minary, J. A. Morrone, D. A. Yarne, M. E. Tuckerman, and G. J. Martyna, J. Chem. Phys. **121**(23), 11949 (2004).
- ¹¹P. Mináry, M. E. Tuckerman, K. A. Pihakari, and G. J. Martyna, J. Chem. Phys. 116(13), 5351 (2002).
- ¹²D. A. Yarne, M. E. Tuckerman, and G. J. Martyna, J. Chem. Phys. 115(8), 3531 (2001).
- ¹³ I. C. Tung, A. Krishnamoorthy, S. Sadasivam, H. Zhou, Q. Zhang, K. L. Seyler, G. Clark, E. M. Mannebach, C. Nyby, F. Ernst, D. Zhu, J. M. Glownia, M. E. Kozina, S. Song, S. Nelson, H. Kumazoe, F. Shimojo, R. K. Kalia, P. Vashishta, P. Darancet, T. F. Heinz, A. Nakano, X. Xu, A. M. Lindenberg, and H. Wen, Nat. Photonics 13(6), 425 (2019).
- ¹⁴N. H. Hong, J. Sakai, N. Poirot, and V. Brizé, *Phys. Rev. B* **73**(13), 132404 (2006).
- ¹⁵H. Choi, E. Stathatos, and D. D. Dionysiou, Appl. Catal., B. **63**(1-2), 60 (2006).
- ¹⁶W. I. Park, D. H. Kim, S. W. Jung, and G.-C. Yi, Appl. Phys. Lett. 80(22), 4232 (2002).
- ¹⁷P. Umari and A. Pasquarello, AIP Conf. Proc. **677**(1), 269 (2003).
- ¹⁸P. Umari and A. Pasquarello, Phys. Rev. Lett. **89**(15), 157602 (2002).
- ¹⁹B. Lou, N. Zhao, M. Minkov, C. Guo, M. Orenstein, and S. Fan, Phys. Rev. Lett. 126(13), 136101 (2021).
- ²⁰P. Kumar, J. Lynch, B. Song, H. Ling, F. Barrera, K. Kisslinger, H. Zhang, S. B. Anantharaman, J. Digani, H. Zhu, T. H. Choudhury, C. McAleese, X. Wang, B. R. Conran, O. Whear, M. J. Motala, M. Snure, C. Muratore, J. M. Redwing, N. R. Glavin, E. A. Stach, A. R. Davoyan, and D. Jariwala, Nat. Nanotechnol. 17(2), 182 (2022).
- ²¹D. Lu, D. J. Baek, S. S. Hong, L. F. Kourkoutis, Y. Hikita, and H. Y. Hwang, Nat. Mater. 15(12), 1255 (2016).

- ²²S. Fukushima, S. Tiwari, H. Kumazoe, R. K. Kalia, A. Nakano, F. Shimojo, and P. Vashishta, AIP Adv. 9(4), 045022 (2019).
- ²³I. Souza, J. Iniguez, and D. Vanderbilt, Phys. Rev. Lett. **89**(11), 117602 (2002).
- ²⁴R. Resta, Phys. Rev. Lett. **80**(9), 1800 (1998).
- ²⁵P. E. Blöchl, Phys. Rev. B **50**(24), 17953 (1994).
- ²⁶G. Kresse and D. Joubert, Phys. Rev. B **59**(3), 1758 (1999).
- 27J. P. Perdew, K. Burke, and M. Ernzerhof, Phys. Rev. Lett. 77(18), 3865 (1996).
- ²⁸J. Fontanella, C. Andeen, and D. Schuele, J. Appl. Phys. **45**(7), 2852 (1974).
- ²⁹M. Schubert, T. E. Tiwald, and C. M. Herzinger, Phys. Rev. B 61(12), 8187 (2000).
- ³⁰Y. Etinger-Geller, E. Zoubenko, M. Baskin, L. Kornblum, and B. Pokroy, J. Appl. Phys. 125(18), 185302 (2019).
- ³¹M. D. Groner, J. W. Elam, F. H. Fabreguette, and S. M. George, Thin Solid Films 413(1), 186 (2002).
- ³²D. A. Buchanan, E. P. Gusev, E. Cartier, H. Okorn-Schmidt, K. Rim, M. A. Gribelyuk, A. Mocuta, A. Ajmera, M. Copel, S. Guha, N. Bojarczuk, A. Callegari, C. D. Emic, P. Kozlowski, K. Chan, R. J. Fleming, P. C. Jamison, I. Brown, and R. Arndt, in the International Electron Devices Meeting 2000, Technical Digest, IEDM (Cat. No.00CH37138) (IEDM, 2000).
- ⁵³S. Jakschik, U. Schroeder, T. Hecht, M. Gutsche, H. Seidl, and J. W. Bartha, Thin Solid Films 425(1), 216 (2003).
- ³⁴F. Basso Basset, F. Salusti, L. Schweickert, M. B. Rota, D. Tedeschi, S. F. Covre da Silva, E. Roccia, V. Zwiller, K. D. Jöns, A. Rastelli, and R. Trotta, Quantum Information 7(1), 7 (2001).
- 35M. Upadhyay, M. Ben Elbahri, M. Mezhoud, R. Coq Germanicus, and U. Lüders, Solid-State Electronics 186, 108070 (2021).